International Journal of Bifurcation and Chaos, Vol. 11, No. 4 (2001) 881–902

THE IMPACT OF NONLINEAR DYNAMICS IN THE ATMOSPHERIC SCIENCES

A. A. TSONIS
Department of Mathematical Sciences,
Atmospheric Sciences Group,
University of Wisconsin-Milwaukee,
Milwaukee, WI 53201-0413, USA

Received January 12, 2001

In this review some of the achievements in atmospheric sciences that resulted from chaos theory and its implications are discussed. They include El Niño dynamics, physics and spatiotemporal dynamics of the general circulation, and ensemble forecasting.

1. Introduction

Chaotic dynamical systems possess attractors (limit sets on which the evolution from an initial condition is confined) that are fractal objects and whose Haussdorf–Besicovitch (or fractal) dimension is smaller than the Euclidean dimension of the system's state space. A fractal object, unlike Euclidean objects, possesses no characteristic sizes or length scales [Mandelbrot, 1983]. It displays detailed structure on all length scales. As a result of this characteristic, a fractal set has strange properties such as infinite boundaries enclosing finite areas. This allows motions in state space which correspond to trajectories that have infinite length but are confined on finite areas. Such trajectories represent nonperiodic evolutions that often resemble pure random processes.

The fractal nature of an attractor does not only imply nonperiodic orbits, it also causes nearby trajectories to diverge. As with all attractors, trajectories initiated from different initial conditions soon reach the attracting set, but two nearby trajectories do not stay close. They soon diverge and follow totally different paths on the attractor. This divergence is measured by the positive Lyapunov exponents of the system. Lyapunov exponents give the rate at which nearby trajectories diverge (positive exponents) or converge (negative exponents). For example, the Lorenz system [Lorenz, 1963] has one positive Lyapunov exponent equal to 2.16 bits/s. This is interpreted as follows: if an initial point is specified with an accuracy of one part per million (20 bits) its future behavior could not be predicted after about 9 s [20 bits/(2.16 bits/s)] corresponding to about 20 orbits.

Since the system is deterministic, if one knows the initial condition exactly, it is possible to follow the corresponding trajectory and basically predict the evolution of the system forever. Thus, determinism *exists* in chaotic systems. The problem is that we almost never have perfect knowledge of the initial condition. There will always be some deviation between the measured and actual initial conditions. They may be very close to each other, but they will not be the same. Thus, even though we may know the laws that govern the evolution of the system exactly, the state of the system at a later time can be totally different from the one predicted by the equations thanks to the underlying structure of the attractor. Initial errors are amplified and predictability is limited. Furthermore, even if we know the initial condition perfectly, exact computation for long times requires computing values with more and more digits, which soon becomes

practically impossible. Thus, at some point truncation or round-off error takes place, which introduces a small error that will grow and again lead to unpredictability. Despite these limitations, the discovery of such dynamical systems led to the realization that what appears as random looking can actually be the result of low dimensional deterministic dynamics, and that chaos can provide a new framework to explain and describe complex behavior and to define the limits of predictability of natural systems. This was so appealing to scientists in many fields, that chaos theory and nonlinear science developed rapidly in the last two decades and led to many important insight about how nature works. Here we will discuss some of the major advances in atmospheric sciences.

2. Probing the Dynamics

If the mathematical formulation of a dynamical system is known, then its state space is known and investigating the properties of that system is straightforward. If the mathematical formulation is unknown or incomplete, then the attractor may be reconstructed from an observable (time series) of the system. The reconstruction is achieved by taking a scalar time series $x(t)$ and its successive time shifts (delays) as coordinates of a vector time series given by:

$$\mathbf{X}(t) = \{x(t),\, x(t+\tau), \ldots,\, x(t+(n-1)\tau\} \quad (1)$$

where n is the dimension of the vector $\mathbf{X}(t)$ (often referred to as the embedding dimension) and τ is an appropriate delay [Packard *et al.*, 1980; Ruelle, 1981; Takens, 1981]. For proper reconstructions the embedding dimension n should be equal or greater to $2D+1$, where D is the dimension of the manifold containing the attractor. Such an embedding preserves the topological properties of the attractor. More specifically the embedding will be a diffeomorphism, a differentiable mapping with differentiable inverse from the true phase space to the delay space. This is Whitney's theorem and, strictly speaking, is valid only when we have an infinite and dense set at our disposal. When we only have a limited data set, the theorem may not be valid. In fact, in those cases the word embedding is used loosely as any topologist will argue.

Since the dimension of the attractor is not known *a priori*, the embedding dimension must vary until we "tune" to a structure (attractor) whose characteristics (dimension, for example) become invariant in higher embedding dimensions (an indication that extra variables are not needed to explain the dynamics of the system in question). Once we have the correct embedding dimension, we can then proceed with estimating dimensions, Lyapunov exponents, and perform nonlinear prediction:

- The most common approach to infer the dimension of an underlying attractor is by estimating the correlation dimension. According to this approach [Grassberger & Procaccia, 1983a, 1983b], given a cloud of points in some embedding dimension n, one finds the number of pairs $N(r,\, n)$ with distances less than a distance r. In this case, if for significantly small r, we find that:

$$N(r,\, n) \propto r^{d_2}\,, \quad (2)$$

  then the scaling exponent d_2 is the correlation dimension of the attractor for that n. Since the dimension of the underlying attractor is not known, we test the power law of Eq. (2) for increasing values of n and check for a saturation value D_2, which will be an estimation of the correlation dimension of the attractor.
- The Lyapunov exponents measure the rate at which nearby trajectories in phase space diverge or converge. Positive Lyapunov exponents indicate divergence and therefore chaos. In theory the Lyapunov exponents λ_i are defined according to:

$$\lambda_i = \lim_{T\to\infty} \frac{1}{T} \int_0^T dt \frac{d}{dt} \ln\left[\frac{p_i(t)}{p_i(0)}\right]$$

$$= \lim_{T\to\infty} \frac{1}{T} \ln\left[\frac{p_i(T)}{p_i(0)}\right] \quad (3)$$

  Here $p_i(0)$ is the radius of the principal axis p_i at $t=0$ of an initial hypersphere of dimension n and $p_i(T)$ is its radius after a long time T. The dimension n is the dimension of the Euclidean phase space in which the attractor is embedded. There are as many Lyapunov exponents as the dimension of the phase space.

  The estimation of the Lyapunov exponents from a system of ordinary differential equations is straightforward and it is based on the fact that the linearized equations which describe the local dynamics involve a Jacobian whose eigenvalues provide all the exponents (see [Tsonis, 1992]). In practice (i.e. from an observable), at first we

embed the data in some space whose dimension is sufficient (normally $d_e > 2D$). Then the reconstructed phase space provides the information to estimate the Jacobian by monitoring the motion in space of selected points and their neighborhoods [Abarbanel & Kennel, 1991].

Because the linearized equations provide the local dynamics such an approach provides an estimation of the local Lyapunov exponents. By repeating the procedure for many points, we can obtain an average picture which will be related to the average Lyapunov exponents of the system.

- Chaotic systems obey certain rules. Their limited predictive power is due to their sensitivity to initial conditions and to the fact that we cannot make perfect measurements. However, before their predictive power is lost (i.e. for short time scales) their predictability may be quite adequate and possibly better than the predictive power of linear statistical forecasting. The philosophy behind nonlinear forecasting is to explore the dynamics in order to improve predictions and to identify nonlinearities in the data.

Since we need to explain the dynamics, we need to have the reconstructed attractor. Then we can begin to think how to improve short-term prediction. If an underlying deterministic mechanism exists, then the order with which the points appear in the attractor will also be deterministic. Thus, if we somehow are able to extract the rules that determine where the next point will be located in phase space we will obtain a very accurate prediction. In general, we can assume that the underlying dynamics can be written as a map f of the form

$$x(t+T) = f_T(x(t))\,,$$

where in state space $x(t)$ is the current state and $x(t+T)$ is the state after some time interval T. However, in reality we cannot easily find the actual form of function f. A solution to this problem is an approach called the local linear approximation [Farmer & Sidorowich, 1987]. According to this approach, the future state is determined by a linear mapping that applies to the evolution of a small neighborhood around the current state. Since the linear mapping may not be the same at each time step the overall procedure is not linear. Nonlinear prediction, unlike other methods for identifying chaos, maximizes the information in the available data and thus often works well with small data sets [Sugihara & May, 1990; Elsner & Tsonis, 1992]. Calculation of the correlation dimension, for example, is based on the estimation of the scaling region which is typically small, thus exploiting only a small subset of the available points in the phase space. Nonlinear prediction uses all the available data, thus requiring smaller samples. For that reason, nonlinear prediction became a popular alternative to dimension estimates and a common tool in nonlinear time series prediction, not only in atmospheric sciences but in many other disciplines (for more information on nonlinear prediction see [Tsonis, 1992]).

Note that proper reconstruction has to overcome several problems with the most important one being the sample size (number of points on the reconstructed attractor). The details behind these estimation procedures and their problems are not of interest here. They are published in numerous papers and books (see for example, [Tsonis, 1992; Tsonis *et al.*, 1994], and references therein). For this reason we will avoid here a lengthy discussion on these issues. Rather, we will proceed with reported results and their interpretation.

3. Are there Low Dimensional Attractors in Weather and Climate?

The first calculations that were reported were dimension estimates from observables. These observables represented dynamics over different time scales, ranging for very long (thousands of years) [Nicolis & Nicolis, 1984] to very short (hours) [Tsonis, 1988]. Virtually every report suggested a low dimensional attractor of dimension between 3–8. These dimension estimates stirred a lot of excitement as they suggested that a system as complex as climate could be described by just a few equations. After the first excitement, came (as usual) controversy as almost all of the estimates were contested as wrong. The major problem seemed to be that in all of these studies the sample size was simply too small. While this issue has been debated extensively [Smith, 1988; Nerenberg & Essex, 1990; Tsonis *et al.*, 1994], it has not been settled beyond doubts.

In a sense, it is naive to imagine that our climate (a spatially extended system of infinite dimensional state space) is described by a grand

attractor let alone a low dimensional attractor. If that were the case, then all observables representing different processes should have the same dimension, which is not suggested from the myriad of reported dimensions. In [Tsonis & Elsner, 1989], it was suggested that if low dimensional attractors exist they are associated with subsystems each operating at different space/time scales. In his study on dimension estimates, Lorenz [1991] concurs with the suggestion of Tsonis and Elsner [1989]. These subsystems are usually nonlinear and may exhibit a variety of stable periodic (equilibrium attractors) or chaotic (nonequilibrium attractors) behaviors. All subsystems are connected with each other, as in a web, with various degrees of connectivity. Accordingly, any system can transmit "information" to another system thus perturbing its behavior. This "information" plays the role of an ever present external noise which perturbs the behavior of the system. Depending on the connectivity of the system to the other systems, the effect can be dramatic or negligible. Systems with weak connectivities will be approximately "independent", and as such they may exhibit low dimensional chaos depending on the parameters involved. Nonlinearity and imperfect initial conditions will make these systems unpredictable after some time. Identification of these subsystems thus becomes important, since it allows us to treat these systems as isolated or closed systems. Otherwise, low dimensional chaos will not be favored. Unfortunately, it is not known *a priori* that a particular observable represents a weakly-coupled subsystem, and, thus, often the procedure and interpretation of the resulting calculation of the attractor dimension is not valid. Therefore, we should not be surprised if a low dimensional system exists somewhere in nature. But we should not expect low dimensional chaos everywhere (see also [Tsonis, 1996]).

Given the above, the question arises. If subsystems exist in the climate system what are they and what physics can we infer from them?

4. Possible Subsystems in the Climate System

4.1. *The El Niño/southern oscillation (ENSO)*

Extended periods of anomalously warm sea surface temperature occurring aperiodically off the coast of South America are called El Niño events. This warming results in a complex interaction with the atmosphere. Under normal conditions the southern hemisphere trade winds, which flow from east to west, drive warm surface water westward causing higher temperatures and even an increase in sea level in the western Pacific than in the eastern Pacific. Warmer water in the western Pacific leads to higher air temperatures, lower surface pressure, and increased precipitation (due to the increase in convection). If the trade winds diminish El Niño develops. The warm water normally found in the western Pacific "sloshes" eastward and gradually makes its way to the coast of equatorial and South America. Eastward surface flow is enhanced by changes in atmospheric convection, which shifts eastward with the warmer water, intensifying westerly wind anomalies and strengthening the tendency of water to flow eastward. These changes are linked to the atmospheric zonal circulation in this region, with atmospheric pressure increasing over western Pacific and dropping over eastern Pacific. This pattern of reversing surface air pressure at opposite ends of the Pacific Ocean is called the Southern Oscillation. Because the ocean warming and the pressure reversals occur rather simultaneously, the whole phenomenon is called El Niño/Southern Oscillation (ENSO). When an ENSO event dies out, the tendency is for the trade winds to return to normal. If, however, they become too strong, then

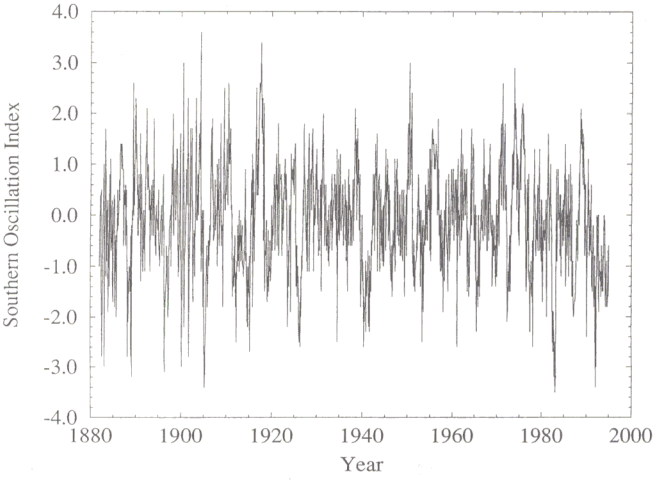

Fig. 1. Time series of the normalized monthly mean sea-level pressure difference between Tahiti and Darwin. The record reveals aperiodic fluctuations in the atmospheric Walker circulation over the tropical Pacific Ocean and is typically referred to as the Southern Oscillation Index (SOI). The record runs from January 1882 to January 1995 for a total of 1357 values.

the cold water pool normally found in the eastern Pacific stretches more westward than normal and warm water and rainy weather is confined mainly in the western tropical Pacific. This opposite to El Niño extreme is called La Niña.

Since the above described changes occur over a very large area of the planet, they ultimately affect through air–sea interaction the weather in many far away places. For example, it is claimed that El Niños are associated with rainy conditions in the southeastern United States and mild dry conditions in the northeastern United States. Even though one cannot "decouple" ENSO from the rest of the planet it is tempting, if not logical, to assume that ENSO is a distinct subsystem of the climate system operating over time scales between 1–7 years (ENSO occurs aperiodically with an average period of about 4–5 years).

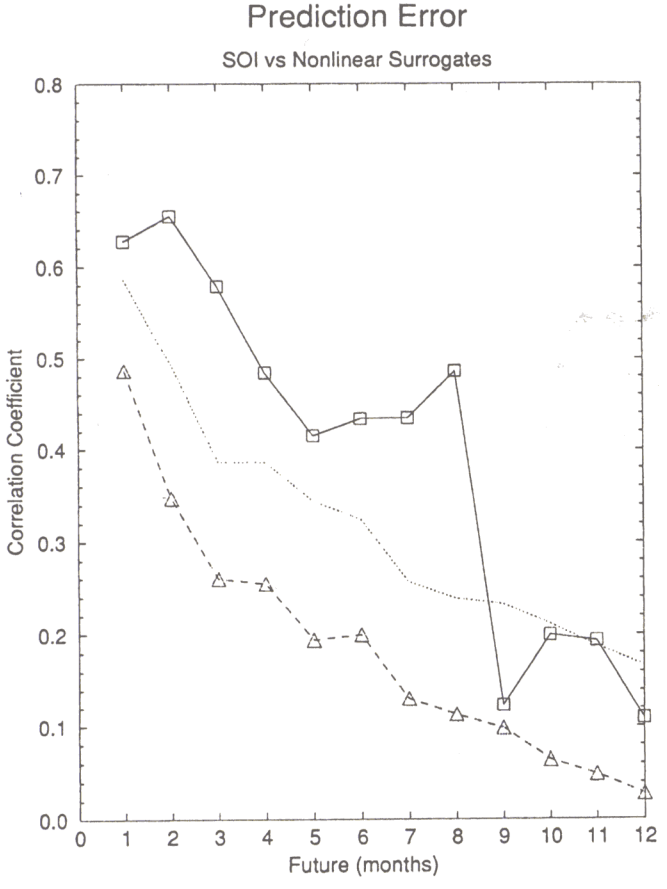

Fig. 2. Correlation coefficient between actual and predicted values as a function of months into the future using a nonlinear prediction algorithm. Solid lines with squares is the function of the original SOI and the dashed line with triangles the mean function of fifty surrogates. The one-standard deviation above that mean is shown by the dotted line. According to the way the surrogates are generated (see [Elsner & Tsonis, 1993]) the null hypothesis is that SOI is a nonlinear transformation of a linear Gaussian process (in this case the surrogates have the same mean, variance and autocorrelation structure). According to these results, the null hypothesis is rejected on the average at about 90% confidence level.

4.1.1. *Nonlinearity in ENSO*

The nonlinear character of ENSO has been empirically investigated extensively using the Southern Oscillation Index (SOI) (Fig. 1). The results (for an example, see Fig. 2), even though based on limited data, consistently indicated that ENSO is a low dimensional chaotic system with a dimension somewhere around six [Hense, 1987; Tsonis & Elsner, 1992; Bauer & Brown, 1992; Elsner & Tsonis, 1993] and with an average predictability limit of about three months [Tsonis & Elsner, 1997]. This low dimensional chaos is consistent with theoretical studies involving simple ENSO models [Tziperman *et al.*, 1994; Vallis, 1986], and with more sophisticated models [Neelin & Latif, 1998] which have indicated that interaction between the annual cycle and the inherent frequency of ENSO leads to frequency-locking and chaos. The transition to chaos takes place primarily along the quasi-periodicity route, which is common in periodically forced nonlinear systems. In general, two parameters are responsible for this scenario. One parameter affects the inherent frequency of the ENSO oscillation relative to the annual cycle, and the other one affects the strength of nonlinearity. As nonlinearity increases, the tendency of the ENSO cycle to lock its frequency on rational fractions of the annual frequency also increases. When the system jumps between the various subharmonic resonances, chaos can ensue (see Fig. 3).

4.1.2. *ENSO and global temperature*

Apart from the annual cycle, it would appear that ENSO is closely related to the global temperature signal. Two such studies have shed light into this very important issue. In the first study [Tsonis & Elsner, 1997], the nonlinear structure of SOI was probed by estimating the local Lyapunov exponents λ_i. The local Lyapunov exponents relate to the divergence of nearby trajectories at a specific location in the attractor and can provide (by adding all the positive exponents) a measure of the predictability of the system along its trajectory in state space (or in other words predictability as a function of time). By embedding the SOI data in a six-dimensional

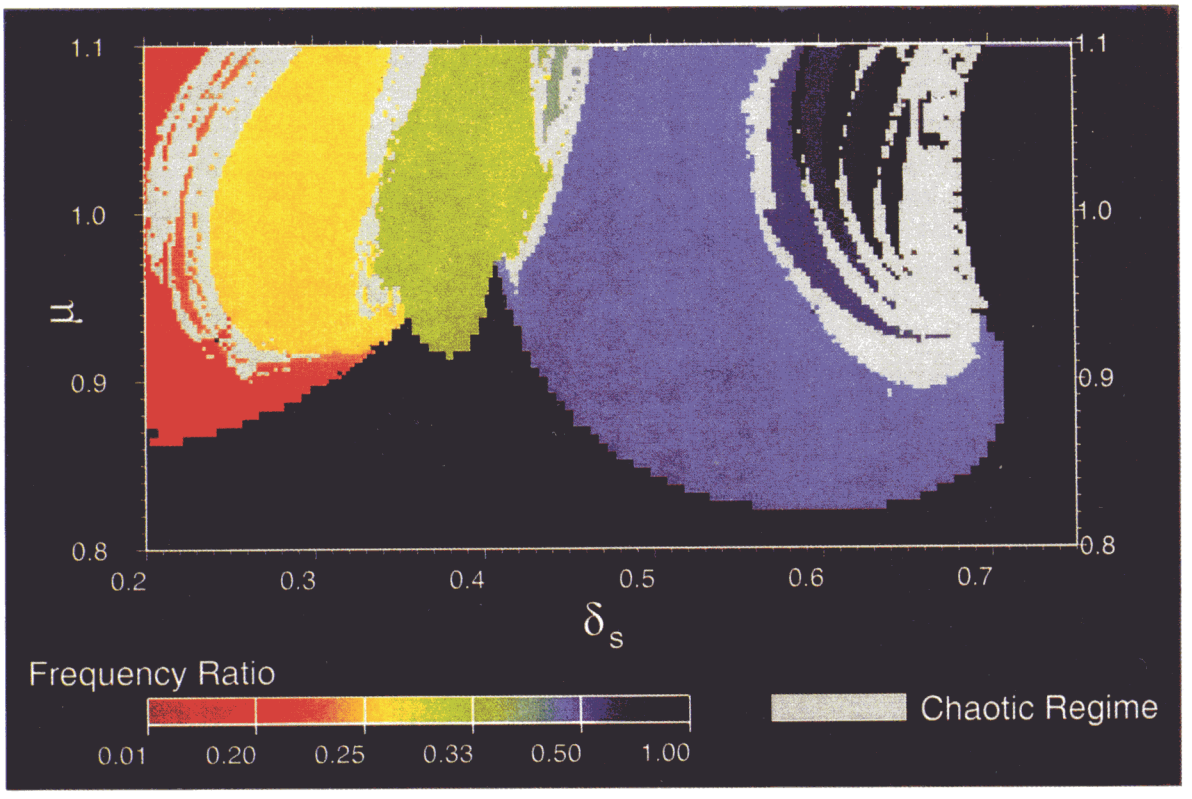

Fig. 3. Dependence of chaotic or frequency-locked behavior on model parameters for an El Niño model from which weather noise has been excluded. The vertical axis is a coupling parameter, which affects the amplitude of the simulated El Niño through the strength of atmospheric wind anomalies. The horizontal axis is a surface-layer parameter, inversely related to the strength of momentum mixing between the surface layer and the layer below. The surface-layer parameter affects the length of the simulated cycle, since stronger currents tend to change surface temperature faster. The plot represents the result of about 3000 500-year simulations, with each simulation classified as chaotic (gray) or frequency locked (color). In the frequency-locked case, color represents the frequency ratio of the El Niño oscillation to that of the annual cycle. For example, 0.33 is one El Niño every three years, while 0.30 is three El Niños every ten years. Ratios of integers occur only for frequency-locked solutions. By contrast, the chaotic solutions occur between the strongly frequency-locked regions, where the solution tends to lock first on one interval and then on the other. (Figure courtesy of Prof. David Neelin.)

space, it was found that for SOI there exist two positive exponents (indicating expansion along two directions) one zero exponent (corresponding to the slowly changing magnitude of the principal axis tangent to the flow) and three negative (indicating contraction along the remaining directions). The sum of the positive Lyapunov exponents is an estimate of the metric (Kolmogorov) entropy, K, and is related to the geometry of the underlying dynamics. The inverse of K is a measure of the predictability of the system. It was found that for the two positive Lyapunov exponents, $\langle\lambda_1\rangle = 0.273$ (months^{-1}) and $\langle\lambda_2\rangle = 0.130$ (months^{-1}), where $\langle\ \rangle$ indicates the average over all locations in the reconstructed attractor. The fact that the two average values are comparable suggests that chaotic dynamics in SOI arise from the interference of two mechanisms of instability of comparable importance. Along the trajectory, the sum $\lambda_1 + \lambda_2$ ranges from a minimum of about 0.3 to a maximum of about 0.5 with $\langle\lambda_1 + \lambda_2\rangle = 0.403$ (months^{-1}). These values put the limits of predictability ($\langle\lambda_1 + \lambda_2\rangle^{-1}$) of the underlying dynamics in SOI (not necessarily of ENSO whose predictability limits are higher) between 2 and 3.3 months. Figure 4 shows $\lambda_1 + \lambda_2$ (or K) as a function of time. The above results were shown to be statistically significant at a 90% confidence level.

A careful examination of Fig. 4 reveals striking similarities with global temperature records as it exhibits an overall positive trend with the following features: a decrease up to about 1905, a steady increase up to about 1940, a subsequent decrease up to about 1970 and a rise afterwards. Such features can be identified in almost all global temperature records as, for example, in the global marine air temperature record [Newell *et al.*, 1989] (Fig. 5).

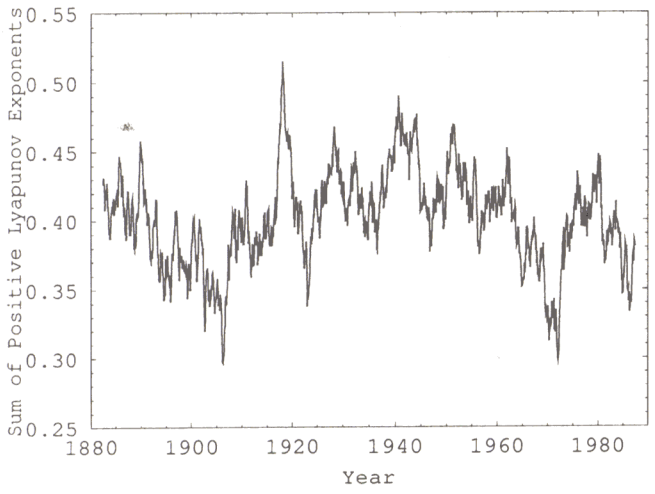

Fig. 4. The sum of the positive Lyapunov exponents (months^{-1}) along the trajectory (or as a function of time) generated by the SOI record. The inverse of this sum is a measure of the predictability of the system (see text for details).

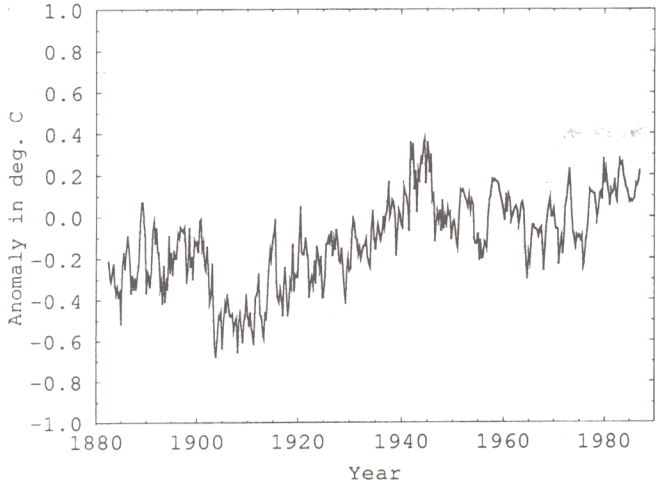

Fig. 5. The annual global marine air temperature record. Comparison with Fig. 4 reveals striking similarities between the two signals. Both series have an overall slight positive trend and segments of similar tendencies.

These two records correlate highly but this could be due to the presence of the overall slight positive trends. If, however, it is found that the detrended series are coherent over a band of frequencies, then it is more likely that the two time series are related. Coherence [Priestley, 1981] is a measure of the linear correlation between two time series over a given frequency band when the phase difference is set to zero. Statistically significant coherence over a frequency band indicates linear relationship between the corresponding oscillatory components. In addition, phase estimates can provide temporal (lead/lag) relationships between the two variables. Thus, coherence estimates and phase relationships can provide useful insights about physical relationships.

Figure 6(a) shows the multiple-window [Thomson, 1982; Kuo *et al.*, 1990] magnitude-squared coherence of the detrended time series transformed by $\tan h^{-1}$. As a compromise between statistical reliability and resolution, a bandwidth of 0.16 cycles/year is adapted, which results in 16 Slepian sequences ($0.16 \times T$) where $T = 105$ is the length of the series in years. On such a scale, coherence estimates are roughly Gaussian with unit standard deviation [Thompson, 1982]. As a consequence, the statistical significance of the coherence between the two series can be made directly. The 80% and 90% confidence levels of this distribution are shown as the two horizontal lines. Remarkably, the two signals have a coherence much above the 90% confidence level at frequencies less than 0.25 cycles/year (i.e. for time scales greater than about four years). Thus, the residuals of the two series are coherent with high confidence over the above low frequency band. At higher frequencies apparently other unknown factors inhibit high coherence. Phase estimates [Fig. 6(b)] show no positive or negative trend suggesting no lead/lag relationships between the two signals. We can thus conclude that warmer temperatures correspond to higher K values or to lower predictability. Therefore, there is significant evidence that global temperature and Kolmogorov entropy, K, are linearly related at all frequencies lower than 0.25 cycles/year. Thus, as the temperature of the planet increases predictability ($1/K$) of the ENSO decreases.

Dynamically speaking we may view global temperature as a controlling factor (input) whose changes modify the dynamics and thus the character of the system, a view consistent with the theory of connected dynamical subsystems discussed earlier.

In the second study nonlinear properties in a global temperature record were examined by probing the fractal properties of the random walk generated by that record. According to random walk analysis, a time series $x(t)$ is mapped onto a walk by calculating the net displacement, $y(t)$, defined by the running sum,

$$y(t) = \sum_{i=1}^{t} x(i)\,. \tag{4}$$

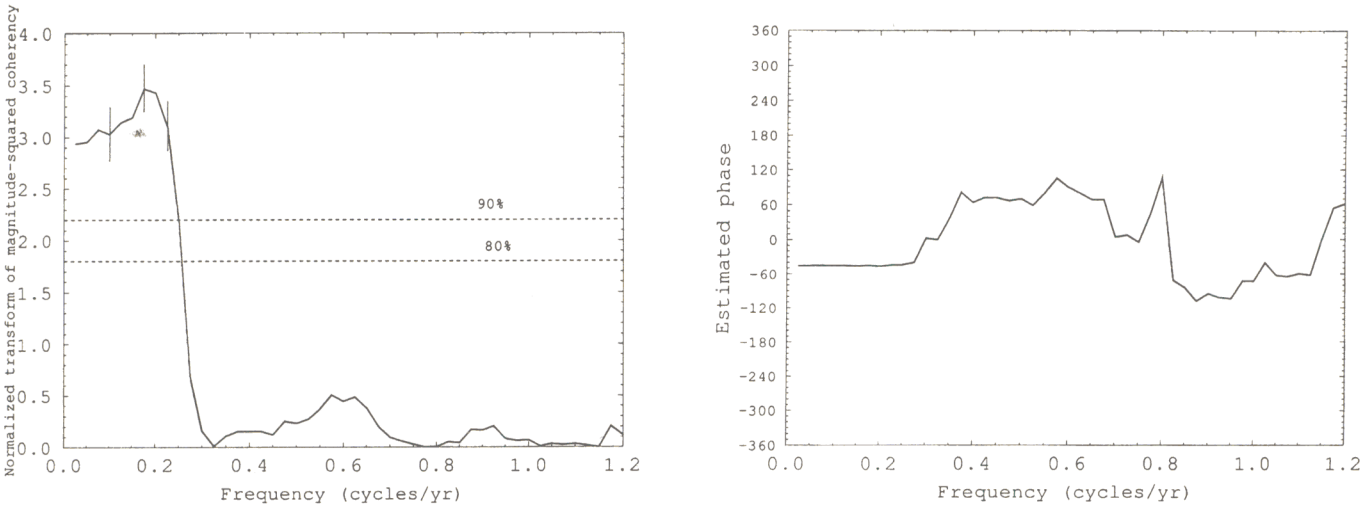

(a) (b)

Fig. 6. (a) Magnitude-squared coherence between the signals in Figs. 4 and 5 transformed by $\tan h^{-1}$. On this scale the values are Gaussian with unit standard deviation. The 80% and 90% confidence levels of this distribution are shown by the parallel broken lines. The bars show one standard deviation of the transformed coherence values as determined by jack-knifing over windows [Kuo *et al.*, 1990] for selected frequencies. (b) Phase of coherence between the two signals. The absence of any significant trends indicate no lead/lag relationships. The graphs are not extended to higher frequencies because the coherence remains almost zero everywhere.

A suitable statistical quantity used to characterize the walk is the root mean square fluctuation about the average displacement,

$$F(t) = [\langle [\Delta y(t)]^2 \rangle - \langle [\Delta y(t)] \rangle^2]^{1/2} \qquad (5)$$

where $\Delta y(t) = y(t_0 + t) - y(t_0)$, and $\langle\ \rangle$ indicates an average over all positions, t_0, in the walk. When $F(t) \propto t^H$, it is possible to distinguish three types of behavior: (1) uncorrelated time series with $H = 0.5$, as expected from the central limit theorem, (2) time series exhibiting positive long-range correlations with $H > 0.5$, and (3) time series exhibiting negative long-range correlations with $H < 0.5$. Markov processes with local correlations extending up to some scale also give $H = 0.5$ for sufficiently large t. It is well known [Feder, 1988] that the correlation function $C(t)$ of future increments, $y(t)$, with past increments, $y(-t)$, is given by $C(t) = 2(2^{2H-1} - 1)$. For $H = 0.5$ we have $C(t) = 0$ as expected, but for $H \neq 0.5$ we have $C(t) \neq 0$ independent of t. This indicates infinitely long correlations and leads to a scale-invariance (scaling) associated with positive long-range correlations for $H > 0.5$ (i.e. an increasing trend in the past implies an increasing trend in the future) and with negative long-range correlations for $H < 0.5$ (i.e. an increasing trend in the past implies a decreasing trend in the future). Note however, that positive long-range correlations do not imply persistence as usually used in climatology, which is defined as the continuance of a specific pattern. Scale invariance is a law that incorporates variability and transitions at all scales in the range over which it holds and is often a result of nonlinear dynamics. Note that long-term trends in $x(t)$ should be removed as they may correspond to processes at time scales longer than the length of the data. In these cases, the inclusion of a long-term trend will make the results trivial.

The actual definition of scaling demands that scaling extends to infinity (space or time). While this is possible in a mathematical sense, it is impractical in physical experiments. Physical systems, like the climate system, have finite size, and are characterized by processes that operate at different space/time scales [Tsonis, 1998]. If these processes are scale invariant, the associated scaling must be limited. In such a framework, certain processes may be characterized by an H greater than 0.5 and thus they may promote a trend. This tendency can take the system away from its equilibrium state. Thus, it is reasonable to assume that if the system remains near equilibrium, processes must be operating at

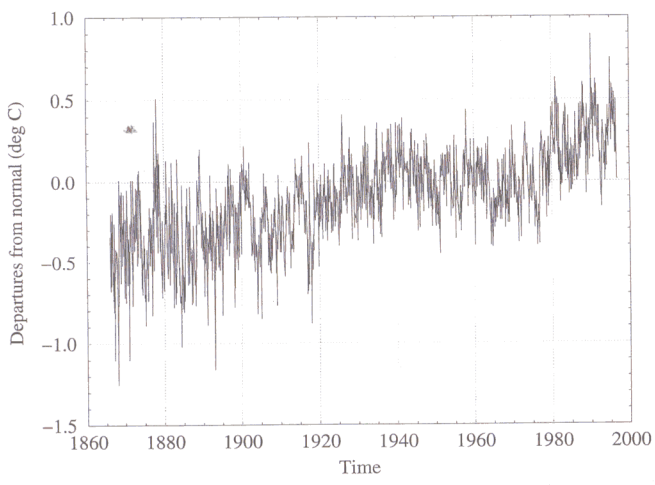

(a)

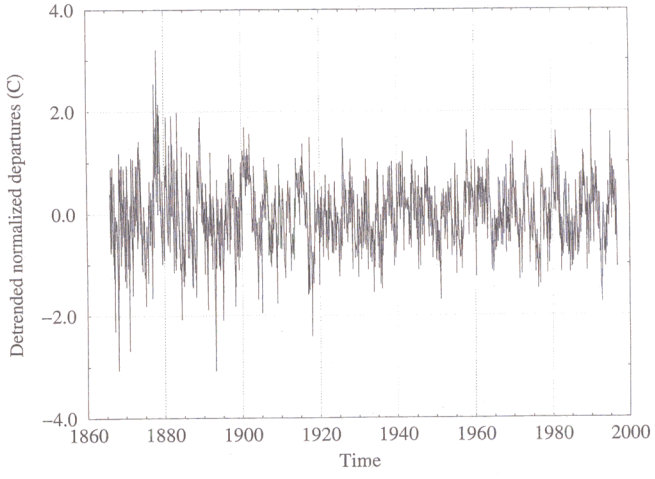

(b)

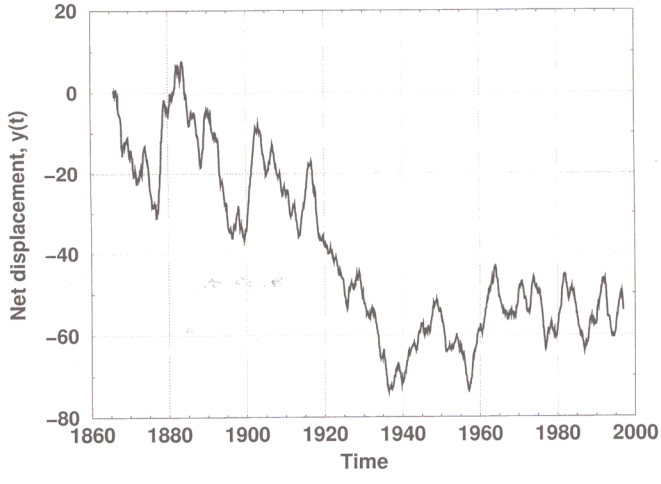

(c)

Fig. 7. (a) The International Panel for Climate Change (IPCC) monthly global temperature anomaly record [Folland *et al.*, 1999]. (b) The detrended monthly global temperature anomaly record, $x(t)$. The trend is removed using singular spectrum analysis (SSA) [Elsner & Tsonis, 1996]. SSA, which is fully nonparametric, considers M lagged copies of a centered time series $Z(t)$ sampled at equal intervals, τ, $Z_i = Z(t_0 + i\tau)$, $i = 1, N$, and estimates the eigenvalues, λ_k and eigenvectors, μ_k, of their covariance matrix C (here $1 \leq k \leq M$). The eigenvectors are called empirical orthogonal functions (EOFs) and the coefficients, α_k, involved in the expansion of each lagged copy, principal components (PCs). As a result of the orthogonality requirement, each principal component can be isolated and probed independently of the remainder of the time series. Accordingly, the time series can be reconstructed to include any subset of the principal components. The removal of one or more of the components is therefore a form of filtering. Usually, the first PCs correspond to ultra-low oscillations or trends. Thus, reconstructing the record by successively removing the leading PCs may result in a nonparametric trend removal. The number of leading PCs that should be removed in order to remain with a record of zero slope is decided by employing the nonparametric test of Kendall and Stuart [1977]. For the temperature data $N = 1572$, and it was assumed that $M = 350$. It was found that the first three PCs need to be removed before the reconstructed record from the remaining PCs has a trend that is statistically insignificantly different than zero (at a significance level of 0.01). (c) The net displacement, $y(t)$, of the random walk based on the data in 7(b).

other time scales in order to avoid a runaway effect. Under this scenario we should be able to discover characteristic space or time scales associated with these mechanisms. Such characteristic scales provide useful insights about the system, which may enhance its predictability. The mapping of a time series to a random walk and the subsequent analysis provide an elegant way to search for characteristic

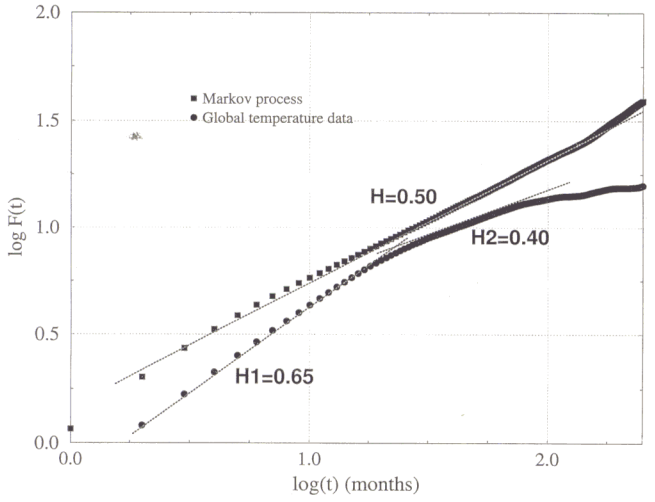

Fig. 8. The log–log plot of $F(t)$ versus t of the displacement shown in Fig. 7(c). The circles correspond to the temperature data and the squares to a surrogate Markov process of the same length and lag-one autocorrelation. The temperature data exhibit double scaling whereas the stochastic data exhibit one scaling region as expected from theory.

time scales in data, as demonstrated next for global temperatures.

Figure 7(a) shows the actual global monthly temperature anomaly record [Follard *et al.*, 1990], and Fig. 7(b) the detrended anomaly record, $x(t)$. Figure 7(c) shows the net displacement, $y(t)$, as a function of time. Figure 8 (circles) is a log–log plot of $F(t)$ versus t for $1 \leq \log t \leq 2.4$ (1 month $\leq t \leq$ 20 years). As t approaches the sample size, the estimation of $F(t)$ involves fewer and fewer points. Thus, extending this type of analysis to longer time scales is not recommended.

The $\log F(t)$ function appears to exhibit two distinct linear regions separated by a small transition region: one in the interval $0 \leq \log t \leq 1.25$ ($1 \leq t \leq 18$ months) and another in the interval $1.35 \leq \log t \leq 1.95$ (22 months $\leq t \leq 7.4$ years). The linear fits over these two regions result in slopes $H_1 = 0.65$ and $H_2 = 0.4$. The correlation coefficient of the linear regression is in both cases greater than 0.99. The null hypothesis H_0: $H_1 = 0.5$ against the alternatives H_a: $H_1 > 0.5$ and the null hypothesis H_0: $H_2 = 0.5$ against the alternative, H_a: $H_2 < 0.5$ are both rejected at a significance level of 0.01. In order to show that the above result is not an artifact of the sample size, a Markov process with the same length and lag one autocorrelation as the temperature data was considered and the analysis was repeated. Now (squares in Fig. 8) the double scaling disappears, and the expected slope of 0.5 is recovered. The two linear regions in the $\log(F)$ function for the temperature data intersect at about $\log t = 1.3$ which corresponds to $t \approx 20$ months. Thus, this analysis indicates that the data in Fig. 7(a) are consistent with a power law with $H_1 = 0.65$ for $t < 20$ months and with a power law with $H_2 = 0.4$ for $t > 20$ months. Alternatively stated, processes of time scales less than 20 months sustain a tendency toward an initial trend (whether positive or negative) and processes of time scales greater than 20 months tend to reverse the past trend. This change in scaling defines an important characteristic time scale in global climate [Tsonis *et al.*, 1998].

The spectra of global temperature data contain significant power at frequencies corresponding to the ENSO cycle (time scales 4–7 years). This result is usually (and correctly) interpreted to imply that ENSO affects global temperatures. While 4–7 years covers most of the scaling range corresponding to negative correlations, the interpretation of the result is complex. As a response to, e.g. a rise in T, El Niño is made more likely. El Niño causes a further increase in T for the next 18 months, or as long as the western Pacific energy source has not been exhausted. Subsequently global temperatures cool off. Repetition of an El Niño at, say, four years, contributes to an oscillatory wave form of the global T record with a period of four years, contributing strongly to $P(f)$ at 1/4/yr. Beyond this, however, increases in T which persist for longer times trigger more frequent El Niños throughout the period.

An important point in understanding a random walk analysis of the global temperatures involves some basic aspects of El Niño physics. The western equatorial and off-equatorial Pacific, in contrast to the east, act as a large thermal reservoir [Neelin *et al.*, 1998]; in this region of the Pacific, SST's are not in equilibrium with the wind stress, as they are in the eastern equatorial Pacific [Schneider *et al.*, 1995]. An El Niño event depletes this storage of heat, largely by spreading the heat over a much broader region of the sea surface, while simultaneously reducing the typical vertical thickness of the warm upper layer. As El Niño matures, the depth to the thermocline diminishes while latent heat is transferred to the atmosphere. After typically about 16 months, when the heat energy is depleted, the El Niño begins to collapse. Thus, any event, which triggers an El Niño tends to raise atmospheric temperatures for up to 16–18 months. Subsequently, however, the heat storage in the

western Pacific is reduced, and it takes generally on the order of two years to replenish, meaning that atmospheric temperatures are then typically reduced. In this light, the above result that atmospheric temperature fluctuations tend to be accentuated over time scales of up to 18 months, while they tend to be self-correcting on time scales of 2–7 years, has only one possible interpretation. For short periods of time, increases in atmospheric temperatures trigger El Niños. The development of an El Niño further increases atmospheric temperatures. After El Niño has run its course, the reduction in stored heat in the equatorial and off-equatorial Pacific leads to a reduction in atmospheric temperatures, and the heat reservoir in the tropical oceans is utilized by the ocean–atmosphere system for self-correction. An analogous argument holds for La Niña.

Further, it is noted that ENSO related data [Trenberth, 1997], show a clear change in the El Niño/La Niña cycle in the middle 1970's. In the interval 1950–1975 (with cooling) La Niña events last longer than El Niño events, and are more common than El Niño. Exactly the opposite is the case in the interval 1975-present (and in the early 20th Century) when global temperatures increased. Thus, a hypothesis consistent with these data and the above results would be that El Niño is activated to reverse positive trends, and La Niña to reverse negative trends. Additional support for this hypothesis is provided by a recent case study suggesting El Niño as a mechanism for the tropics to shed excess heat (UCAR Quarterly, 1997, [Sun & Trenberth, 1998]). According to this study, the continuous pouring of heat into the tropics cannot be sufficiently removed by weather systems and ocean currents. By considering global oceanic and atmospheric heat budgets during the 1986–1987 El Niño, it is suggested that El Niño serves as a release valve for the tropical heat. The above results indicate a role for the ENSO cycle in balancing global temperature.

Although the underlying physical aspects of ENSO are understood well, the irregularity of the cycle is still a subject of intense research. The theory of nonlinear dynamical systems has offered useful insights in this area and toward a better understanding and prediction of one of the most important features of our climate system.

4.2. *The Pacific decadal oscillation (PDO)*

The PDO refers to a pattern of two modes of sea surface temperature (SST) in the Northern Pacific Ocean, one in the northwestern part of the basin, and a smaller one in the eastern tropical part of the basin. One of these modes represents warmer water and the other colder water. It has been suggested that this dipole reverses (warm $\longleftrightarrow$ cold) about every 20-years, and that this reversal has significant effects on the weather over North America. Like in ENSO, it is quite possible that large SST anomalies could through air–sea interaction affect the atmosphere. However, due to lack of long SST anomaly records in the Pacific Ocean, there is simply not enough data to delineate with high confidence a suspected cycle of 20 years. As such, even though the PDO is a good candidate for a subsystem very little is certain at this point about its dynamics.

4.3. *The north Atlantic oscillation (NAO)*

It appears that another oscillation exists over the Atlantic Ocean. This oscillation which is also referred to as the Arctic Oscillation (AO) represents another dipole which alternates between low pressures over polar regions and higher pressures at lower latitudes (warm phase) and the reverse (cold phase). A weaker polar high means cold winter air masses do not penetrate as south as the United States. At the same time, cold air masses are more frequent over Newfoundland and Greenland. The higher pressure at lower latitudes results in stronger westerly flow bringing warm air to Northern Europe. It would appear that the NAO switches phase aperiodically on a time scale of decades. As the PDO, NAO is also a topic that is lately receiving a lot of attention and intense research.

With limitations in the available records, many doubts remain about the validity and the statistical significance of PDO and NAO. Nevertheless, the importance in large-scale shifts over the oceans cannot be ignored. If those oscillations are real features of our climate system, then understanding the interaction between them and the atmosphere may offer dramatic improvements in predicting long-term changes in the atmospheric circulation and hence in regional climate. The next few decades will undoubtedly produce exciting insights into this problem as more data are collected and increasingly sophisticated climate models are developed and investigated.

5. Insights into the Dynamics and Physics of the Atmosphere

5.1. *Spatiotemporal patterns in the extratropical atmospheric circulation*

The atmospheric general circulation often enters into regimes that cause weather anomalies (departure from an average state) to persist over areas of the globe. The variability of these atmospheric circulation anomalies has been investigated using the random walk method described earlier. The results suggest important links between processes over time scales from weeks to decades. The data used are daily 500 hPa values at grid points providing full coverage of the Northern Hemisphere (from 20°N). A 500 hPa value indicates the height of the 500 mb pressure level and it is proportional to the mean temperature of the layer from the surface to the 500 mb level. An example of such a variable for a particular grid point is given in Fig. 9(a). Uninterrupted daily 500 hPa values are available for this point from 1964 to 1988 (total of 9132 values). Figure 9(b) is the net displacement of the random walk generated by the time series in Fig. 9(a), and Fig. 9(c) is the log $F(t)$ versus log t plot.

A linear relationship with a slope $H = 0.625$ is very suggestive here. It was shown [Tsonis *et al.*,

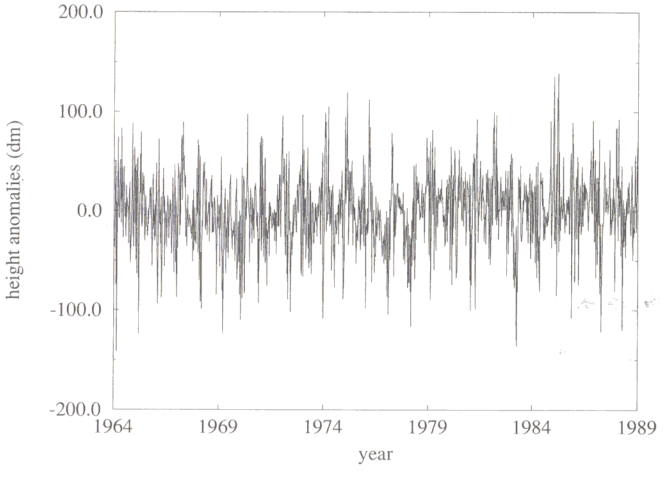

(a)

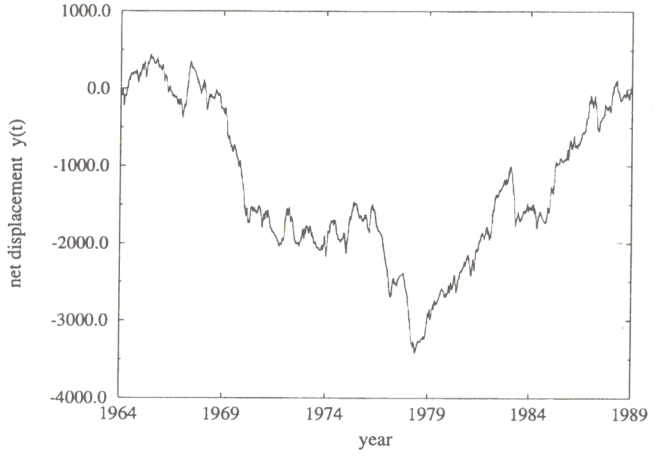

(b)

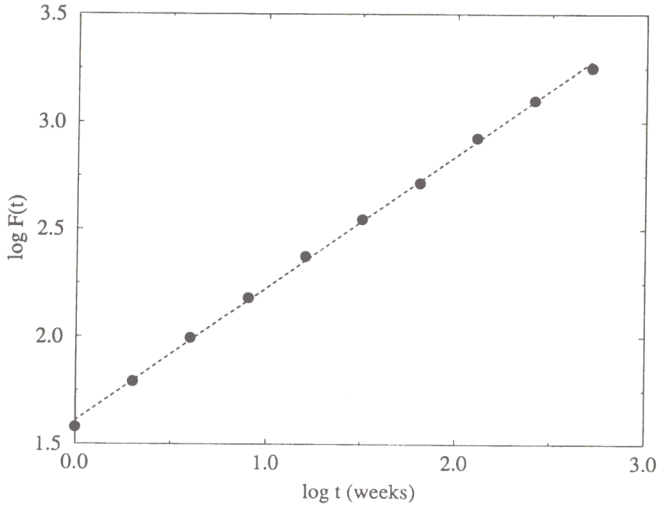

(c)

Fig. 9. (a) The 500 hPa weekly anomaly for grid point 29.7 °N, 86.3°W. (b) The net displacement of the random walk. (c) The log–log plot of $F(t)$ versus t. A linear relationship with a slope of 0.625 emerges. This value indicates positive long-range correlations.

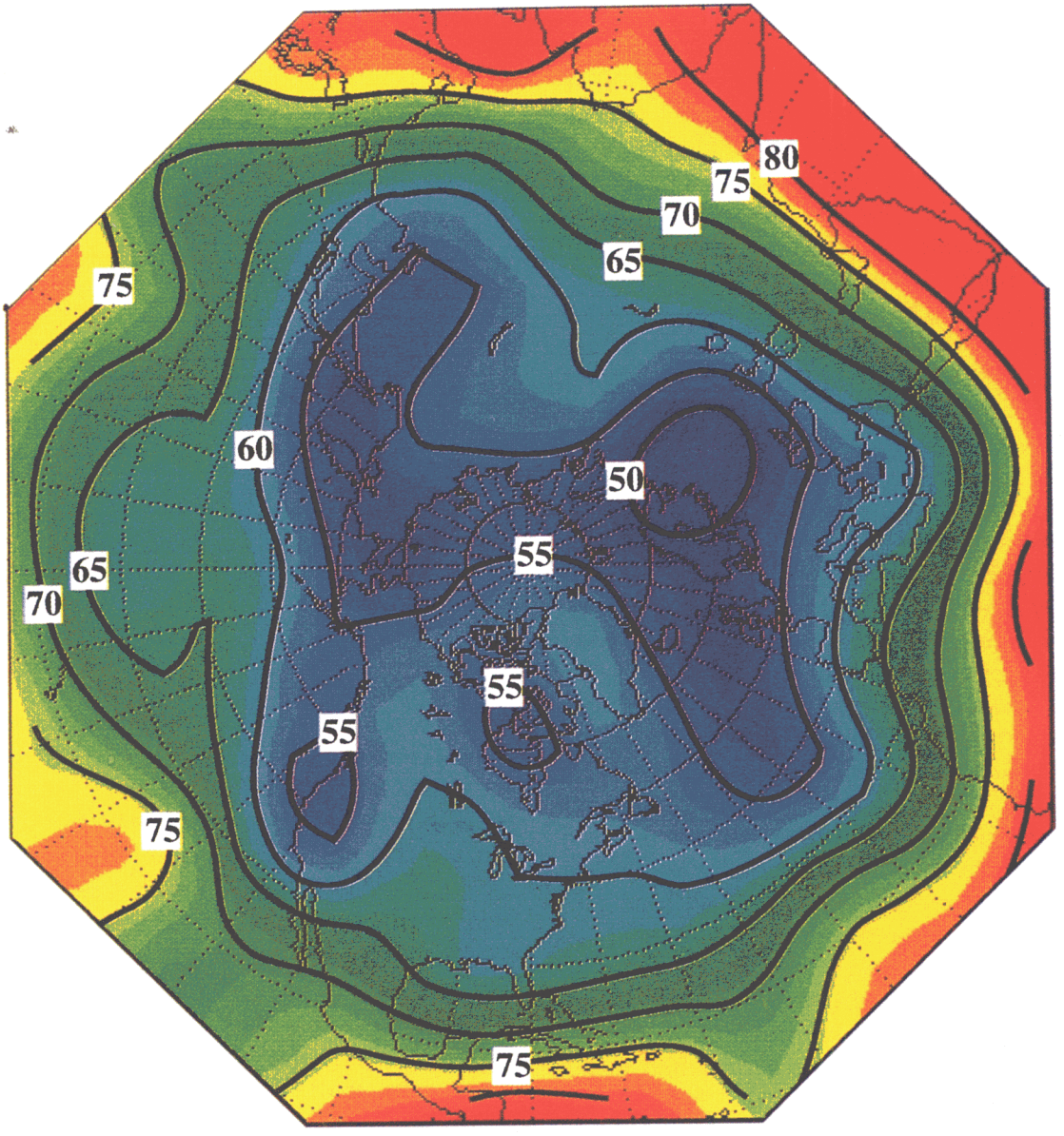

Fig. 10. The spatial distribution of the estimated value of H in the Northern Hemisphere. Warmer (colder) colors indicate higher (lower) values of H. The contour interval is 0.05. Contour labels are plotted with the decimal point removed for clarity. As is explained in the text this result is consistent with large-scale dynamics.

1999] that this scaling is statistically significant at the 98% confidence level. Thus, the results in Fig. 9(c) are strongly suggestive that the anomaly record in Fig. 9(a) exhibits scale invariance in time and positive long-range correlations such that if now a certain type of anomaly (negative or positive) exists it will most likely continue to exist in the future for any $t < 512$ weeks. Otherwise stated, this result would indicate that the dynamical properties of the scaling process at small scales are related to those at large scales via a relationship that involves a magnification factor λ^H, where λ is the ratio of the large time scale to the small time scale.

The generality of this law was then tested by repeating the analysis for all available grid points. The results are shown in Fig. 10 in which the spatial distribution of the exponent H is plotted. Almost everywhere the value of H exceeds 0.5 with a hemispheric mean value of 0.65. Only a small area centered over Finland and the northern reaches of the former Soviet Union appears to exhibit values close to or lower than 0.5 (the lowest value is 0.48). The fact that virtually everywhere the value of H is

greater than 0.5 is a direct consequence of natural processes exhibiting some degree of redness in their spectra (i.e. larger scales possess more energy than smaller scales). We observe a very coherent pattern that is characterized by a general tendency for H to decrease with increasing latitude. This result is consistent with the increasingly baroclinic nature of atmospheric dynamics as one progresses from the subtropics through the midlatitudes (more baroclinicity, more power to small scales, less "redness" in the spectra, smaller exponent H). Variations from this general tendency over the North Pacific and the North Atlantic Oceans are associated with the storm tracks where the influence of very short time scale cyclones and anticyclones is enhanced, resulting in local decreases in H. The consistency of these results with large-scale dynamics and their statistical significance indicate that Fig. 10 would not arise by chance and provide very strong evidence of the universality of long-range correlations in the extratropical circulation.

Tsonis *et al.* [1999] were able to trace this scale invariance to decade-long patterns that are established as a result of the intrinsic variability of the climate system. Their results go further than explaining simple persistence as they indicate that the underlying dynamics and transitions in the atmospheric circulation are associated with a fractal law that dictates that no characteristic timescale exists and that all scales from a week to a decade are connected. A consequence of this law is that the memory of the large scales (low frequency processes) is not independent of the memory of the small scales (high frequency processes). Further, the decrease in H with latitude and the association of low values of H with the Pacific and Atlantic storm tracks shown in Fig. 10, suggest the fundamental role of these high frequency midlatitude weather systems. This would indicate that the memory of the extratropical climate system does not reside only in the oceans (i.e. long time scales) with the atmosphere simply responding passively.

The physics behind the emergence of this scaling are not difficult to produce (Fig. 11). High frequency atmospheric disturbances are crucial agents in achieving the long-term balance of energy, momentum and water vapor in the atmosphere. These systems may also play a fundamental aggregate role in modulating the low frequency (seasonal to decadal) atmospheric flow by communicating the effects of anomalous surface properties (boundary forcing) to the slowly varying

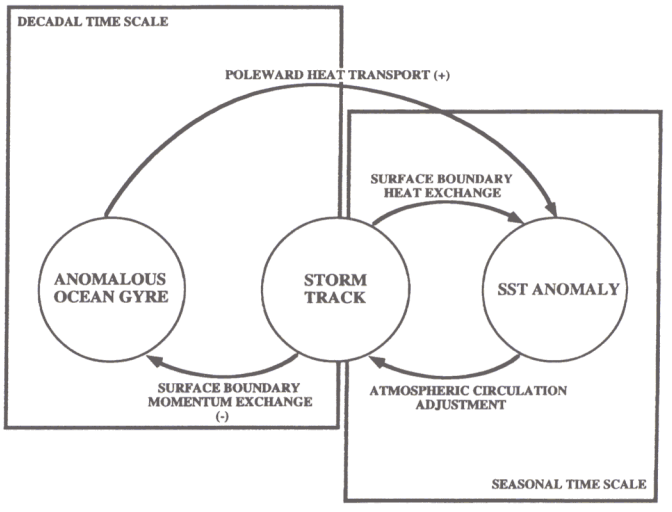

Fig. 11. This diagram presents a scenario according to which long-range correlations in the atmospheric circulation emerge from the interplay of processes operating at time scales ranging from a week to ten years.

components of the climate system. This communication is directly tied to the location of the storm track [Trenberth & Hurrell, 1994]. The position of the storm track largely determines the seasonal distribution of temperature and precipitation, which leads to energetic exchanges of heat and momentum with the underlying surface. It has long been recognized that extratropical sea surface temperatures (SSTs) modulate midlatitude atmospheric variability [Latif & Barnett, 1996; Namias, 1969; Wallace & Jiang, 1987; Lau & Nath, 1990]. Evidence exists to suggest that the atmospheric flow leads the oceanic changes by one to several months [Davis, 1976; Lanzante, 1984; Wallace *et al.*, 1990]; these results indicate that the driving of the ocean by the atmospheric circulation initiates the changes but that once induced, the strong persistence of oceanic SST features feeds back onto the low frequency atmospheric dynamics. The mechanism for this feedback involves oceanic gyre modes (decadal time scale) generated by large-scale atmosphere-ocean interactions in midlatitudes [Latif & Barnett, 1996, 1994; Latif *et al.*, 1996]. Given an anomalous subtropical ocean gyre, adjustments in the oceanic poleward transport of heat will result, leading to midlatitude SST anomalies. These anomalies force an atmospheric response in the form of adjustments in the atmospheric general circulation and associated storm tracks. The aggregate effect of the latter is to modulate both surface heating (reinforcing the existing anomaly) and the wind stress curl

(opposing the sense of the existing oceanic gyre), ultimately readjusting the poleward heat transport and the associated sign of the SST anomalies.

5.2. *Channels of communication between tropics and higher latitudes*

One of the paramount issues in atmospheric sciences is the equatorial to extratropical teleconnections and the interaction between the tropics and higher latitudes. Observational studies [Wallace & Gutzler, 1981; Horel & Wallace, 1981] have established the existence of teleconnections between regions in the tropics and regions in higher latitudes. These teleconnections are attributed to several atmospheric phenomena such as El Niño/Southern Oscillation (ENSO) [Horel & Wallace, 1981], the 40–50 day oscillation [Madden & Julian, 1971, Lau & Chan, 1985], convective activity in the tropics, etc. Theoretical/modeling studies [Hoskins & Karoly, 1981] have suggested and/or speculated on the mechanisms according to which teleconnections might be established. In general, it is proposed that they are established via equatorial Rossby waves (which travel westward) or Kelvin waves (which travel eastward) that are "allowed" to leak northward to higher latitudes. It has been suggested [Wiin-Nielsen & Chen, 1993] that communication between tropics and midlatitudes may be happening through exporting of kinetic energy from low to higher latitudes. What, however, was not settled was the exact location and number of the corridors through which the communication between the tropics and midlatitudes is established.

By applying ideas from information theory and nonlinear prediction, Tsonis and Elsner [1996] were able to empirically obtain an answer to this question. According to Wales [1991], the information loss per unit time in a time series is related to the initial decay of Pearson's correlation coefficient, $r(t)$, between predicted and actual values, provided that the prediction is a dynamic prediction that explores the geometry of the underlying state space (nonlinear prediction). This relationship is given by

$$r(t) = 1 - Ce^{2Kt} \tag{6}$$

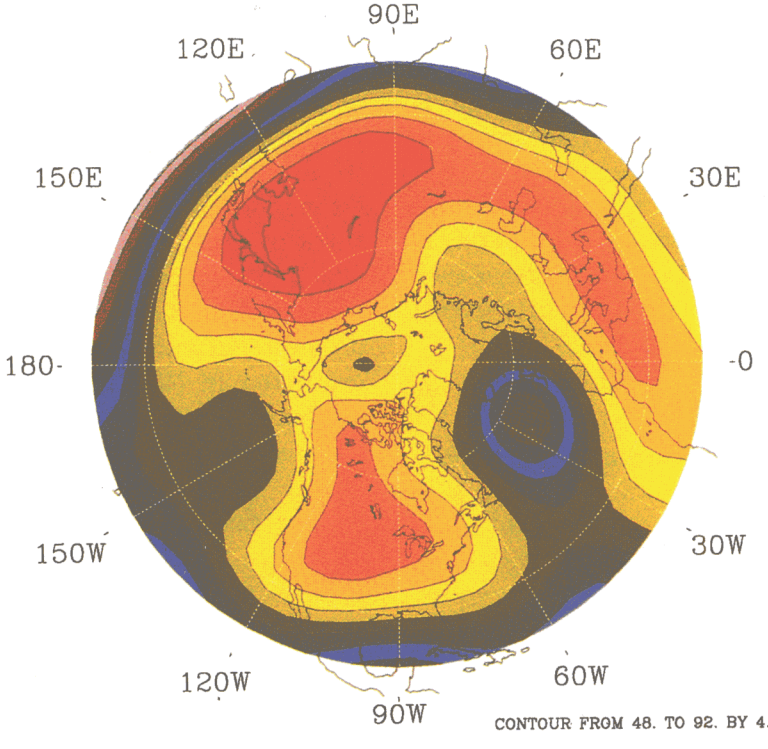

Fig. 12. Spatial distribution of predictability as measured by the quantity $\overline{r}(\times 100)$ (an average correlation between actual and predicted 500 hPa geopotential height values) defined in the text. Correlations range from about 0.5 (violet) to about 0.9 (red). Results have been smoothed using a nine-point uniform filter. Spatial heterogeneity of seasonal to interannual predictability is clearly evident.

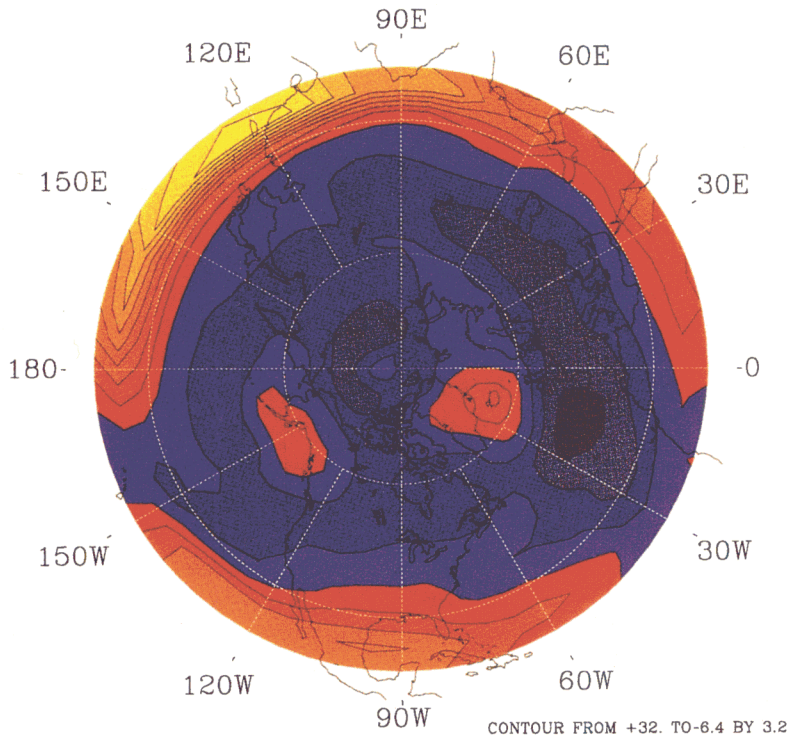

Fig. 13. The north–south gradient of Fig. 12. According to Eq. (7), this map shows regions where the loss of information per distance is fast (i.e. information is not transported easily) [yellow–red] and regions where the loss of information per distance is slow or slightly negative (i.e. information from lower latitudes is transported easier to midlatitudes) [light blue to purple]. Two corridors along which information is transported easily, one over the Pacific Ocean and one over the Atlantic Ocean are evident.

where K is the Kalmogorov entropy, which is related to the information content, I, according to $\dot{I} = -K(K > 0)$. Tsonis and Elsner [1996] showed that the average predictability, $\overline{r}$, over some time interval related to the mean loss of information, $\dot{I}$, over that time interval, and that the north–south gradient of $\overline{r}$ is proportional to the north–south gradient of $\dot{I}$

$$\frac{d\overline{r}}{d\lambda} \propto \frac{d\dot{I}}{d\lambda}, \tag{7}$$

where λ is the latitude. Accordingly, small values of $d\overline{r}/d\lambda$ would correspond to small values of $d\dot{I}/d\lambda$, which will indicate that the rate of information loss per distance is slow. Regions with slow information loss per distance would then represent regions where information flows easier, thereby defining channels along which the communication between north and south is more effective. By considering monthly 500 hPa values in 1080 grid points in the Northern Hemisphere in the period from 1946 to 1989, and performing nonlinear prediction [Farmer & Sidorowich, 1987; Sugihara & May, 1990; Wales, 1991] the spatial distribution of $\overline{r}$ (estimated over a year) was produced. The results are shown in Fig. 12. The high predictability areas over land areas can be explained by the strong dependence of low tropospheric temperatures to changes in solar insolation (annual cycle) which in turn cause drastic changes in atmospheric circulation patterns. The expected low predictability over oceanic regions seems to have been accentuated in Northern Atlantic Ocean where the predictability is much poorer compared to similar regions over Northern Pacific Ocean that normally receive equal amounts of solar insolation. This feature may be attributable to the Gulf Stream and/or to the North Atlantic deep water [Broecker & Denton, 1990]. Both these "signals" give off great amounts of heat in the North Atlantic Ocean thereby making winters over those areas milder. This reduces the amplitude of the seasonal cycle whose predictability drops. Similar comments can be made about the predictability over the subtropical western Pacific Ocean where the values are much lower than those over the subtropical eastern Pacific. This feature is attributable to the seasonal

to inter-annual footprint of the chaotic (and thus unpredictable) ENSO signal.

Figure 13 shows the north–south gradient of $\overline{r}$. Yellow corresponds to $d\overline{r}/d\lambda = 0.34$ which, given the range of $\overline{r}$ in Fig. 12, represents a value significantly greater than zero. As we go from yellow to red, $d\overline{r}/d\lambda$ decreases, approaching zero for light blue and becoming slightly negative for darker blue and purple. From the above discussion and arguments two corridors along which information flows easily (channels of communication) can be identified. One in the Pacific Ocean (centered around 160°W) and a wider one in the Atlantic Ocean (centered around 25°W).

The delineation of these channels of communication provides new insights to our knowledge about large-scale dynamics in the atmosphere. First, their existence verifies model results that have suggested or speculated the existence of such regions, but not the exact location and number [Hoskins & Karoly, 1981]. The existence of the corridors may explain teleconnections since their location determines where information leaks into higher latitudes. For example, according to Fig. 13, El Niño related fluctuations trigger Rossby waves that emanate to higher latitudes at about 160°W longitude. The subsequent interaction between those fluctuations (or the triggered waves) and the general circulation will result in changes of a certain horizontal scale. Since the immediate land areas are those of the United States and Canada those areas are most likely to be affected. We can thus establish teleconnections between El Niño and changes to weather patterns in North America. These results may also explain the observed by the general circulation models phase-locked response at higher latitudes in the northern Pacific Ocean and America. This phase-locking refers to similar responses irrespective of the place of origin and the nature of the fluctuations in the tropics. It is suggested that because the corridor is rather narrow, the fluctuations trigger waves that emanate into higher latitudes more or less from the same region. Thus they transport information at the same location regardless of the source. It is interesting to mention here that recent results on mass exchanges between northern and southern hemispheres take place along these corridor [Carrera & Gyakum, personal communication]. A similar equation to Eq. (7) may be derived for the longitudinal (east–west) gradient of $\overline{r}$. This gradient, however, is very weak (varying from -0.015 to 0.015) indicating the direct and easy communication due to the prevailing zonal circulation. This result indicates that the information gradient has a much greater (more than an order of magnitude) meridional component than a zonal component and thus it is mostly restricted to the meridional direction.

These results depend on retaining the annual cycle in the data. If the annual cycle is removed, the resulted Fig. 12 makes no sense whatsoever as it loses all its structure and climatology and simply shows noise. Since the annual cycle is more pronounced (and thus more predictable) in the mid-latitudes than in the tropics, according to Eq. (7) information has to flow from tropics to higher latitudes. This "direction" seems to be solely due to the annual cycle. Thus, firstly, these results suggest a greater role for the annual cycle in large-scale dynamics that it is traditionally practiced. Secondly, since the delineation of Figs. 12 and 13 is a direct result of how the spatial distribution of the predictability of the annual cycle signal is modified by basically the El Niño and the North Atlantic signals, these results may be suggesting that, to a large degree, global-scale dynamics over the time scales resolved by the available data arise from the interplay of three major signals (or subsystems) annual cycle, El Niño, and the North Atlantic signal. The Pacific Decadal Oscillation is not involved here possibly because of its long time scale.

6. Ensemble Prediction

Chaos has provided a framework to understand and explain fundamental properties of natural systems. One of these fundamental properties is the limited predictability of nonlinear systems caused by the divergence of nearby trajectories in the attractor (or by the presence of positive Lyapunov exponents). Provided that a system has this property, exploring the local structure of the attractor can actually lead to improved predictions. Nonlinear prediction approaches (such as the one discussed earlier) do that and as a result they outperform any other statistical method [Elsner & Tsonis, 1992]. One of the key results in the theory of nonlinear dynamical systems is that divergence of nearby trajectories is not the same everywhere. In other words, the positive Lyapunov exponent(s) along a trajectory vary (recall Fig. 4). Accordingly, predictability along a trajectory varies. This has led to possibly the most important application of chaos in atmospheric

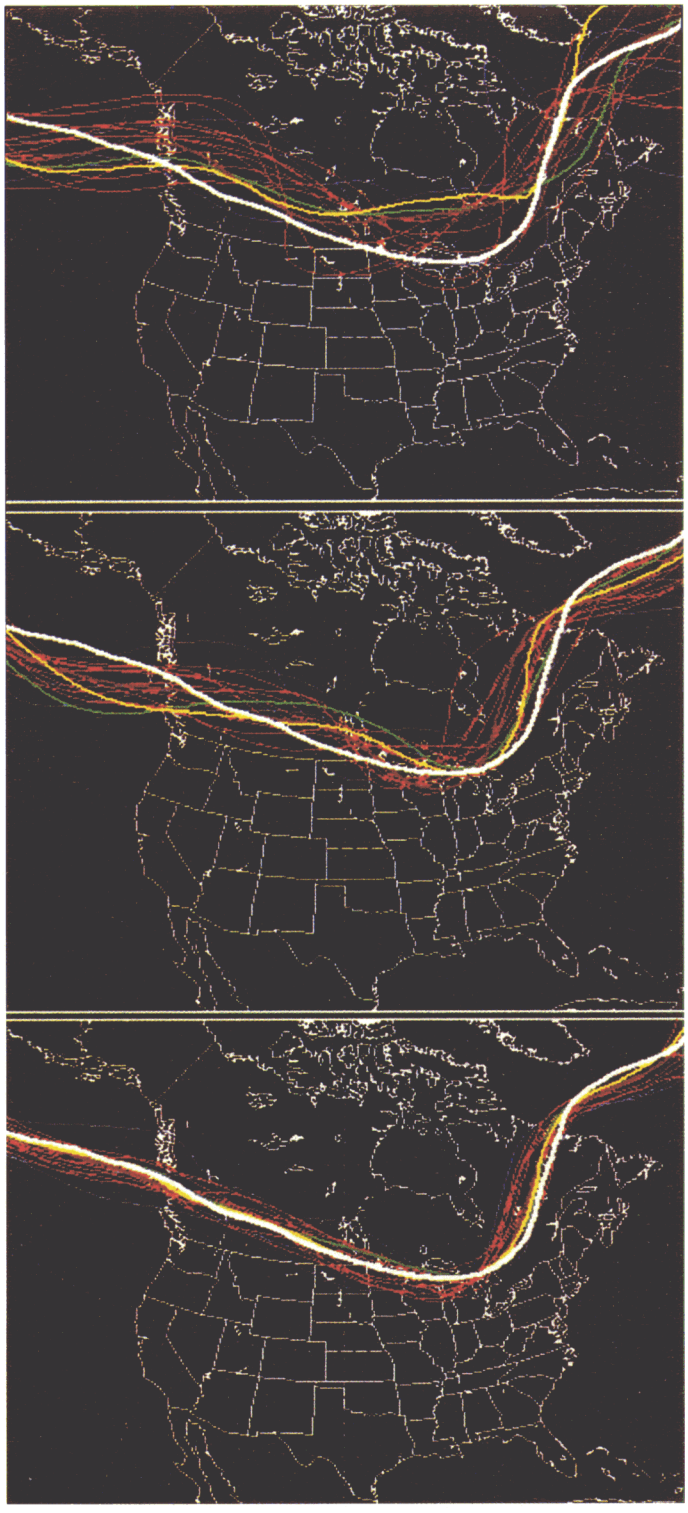

Fig. 14. The individual six-, four-, and two-day forecasts of the 5640 m contour of the 500 hPa height field from an ensemble are shown in the three right panels (from top to bottom). The ensemble consists of 23 forecasts that differ only in that their initial conditions are slightly perturbed in order to represent our uncertain knowledge of the state of the atmosphere. Initial time is 0000 UTC (Coordinated Universal Time) September 13, 2000. The red and blue lines represent the perturbed forecasts whereas the green and yellow lines mark the AVN and MRF control forecasts. Note the large variations in the location and intensity of the trough in the area around the Great Lakes at the longer, six-day lead time. While the control forecasts are relatively poor in this area, there are a number of ensemble forecasts that capture well the true evolution of the atmosphere (white line). The forecast uncertainty is much reduced in the four-, and especially in the two-day forecast. (Figure courtesy of Dr. Zoltan Toth.)

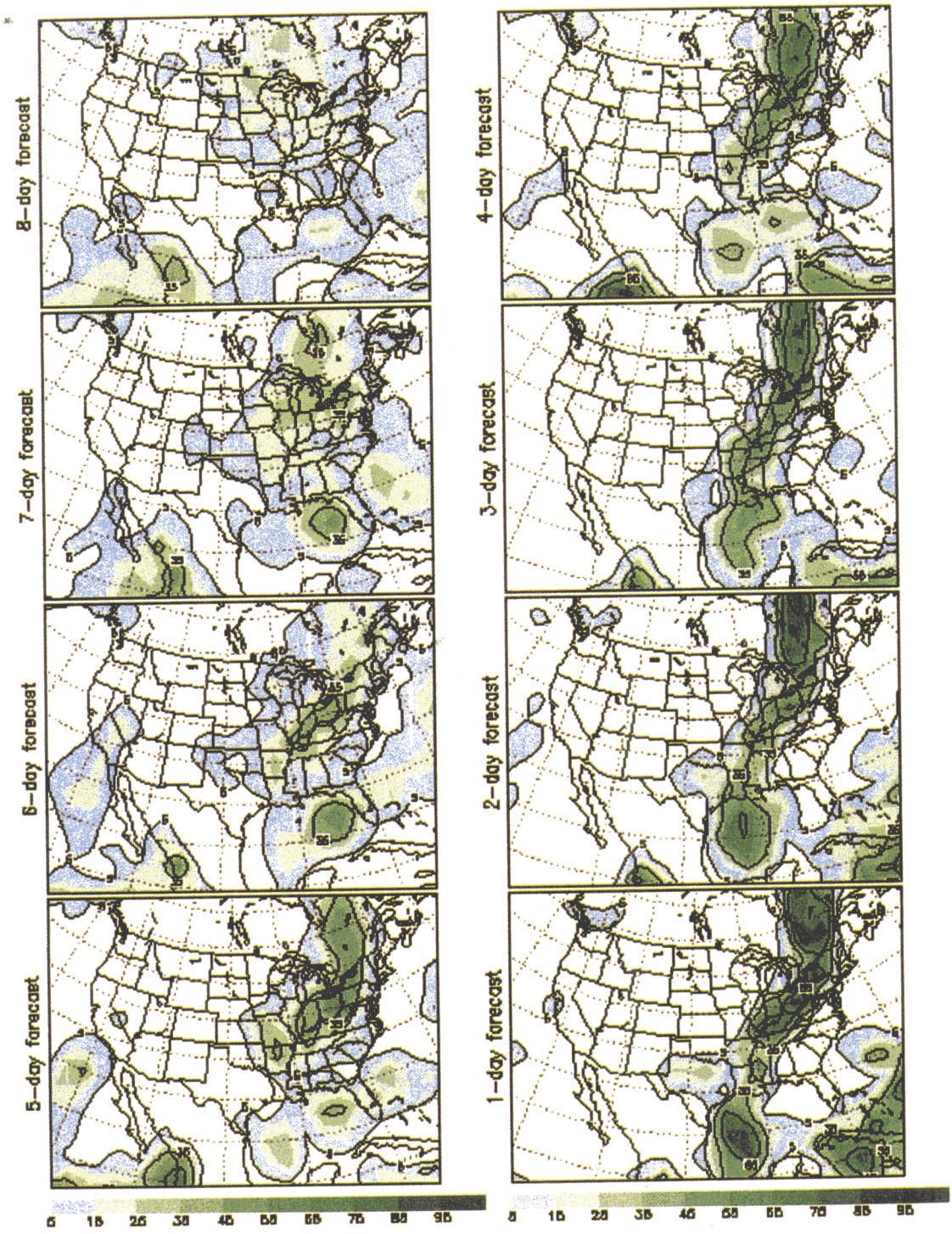

Fig. 15. Each subpanel of the eight-panel figure in the upper left shows the forecast probability of more than half inch of precipitation over a 24-hour period around 0000 UTC September 13, 2000, with lead times, as indicated, from eight to one day. These probabilities are derived from the same ensemble of 23 forecasts in Fig. 14. The high probabilities observed around the Great Lakes area for the longer (six-day or longer) lead times may not be very reliable due to the great uncertainty in location and intensity of the low pressure trough in Fig. 14 over that area and at those lead times. (Figure courtesy of Dr. Zoltan Toth.)

sciences: the ensemble forecasting. The idea behind ensemble forecasting is simple. Make a control forecast starting from some initial state of the climate system (coupled ocean–land–atmosphere system). This results in predicted fields of several variables such as upper level flow (for example, 500 hPa height field), precipitation, temperature, etc. Then, perturb the initial state by a small amount and repeat the forecast. Do this several times to produce an ensemble forecast. If the ensemble members exhibit large spread it means that the system is in an area in the attractor where divergence of nearby trajectories is great. In this case, the forecasts are less reliable than if the spread is small.

While technical details are of no importance here, it should be mentioned that the way the initial state is perturbed is critical. The National Centers for Environmental Prediction (NCEP) in the United States use the so-called breeding method [Toth & Kalnay, 1993, 1995] according to which the initial ensemble perturbations are those that grew faster during the analysis cycle leading to the initial time. The European Centre for Medium-Range Weather Forecasts (ECMWF) uses the singular vector approach [Molteni *et al.*, 1996; Buizza & Palmer, 1995], in which the fastest-growing perturbations are determined for a two-day period at the beginning of the forecast. Figures 14 and 15 show examples of results produced by NCEP. In Fig. 14, the yellow and green lines represent control forecasts of the 5640 m contour of the 500 hPa height field. These control forecasts correspond to two initial states of the climate system, one at 0000 UTC (called MRF) and one twelve hours before (called AVN). The red lines are perturbed MRF forecasts and the blue lines are perturbed AVN forecasts. From bottom to top, the figure shows the two-day, four-day, and six-day lead time forecast of the 5640 m contour. The white line shows the true evolution of the atmosphere. Such diagrams are called "spaggetti" diagrams and help us decide how reliable a forecast is. As we can see in Fig. 14, the individual members of the ensemble exhibit very small spread in the two-day forecast. This spread increases for later times. For the six-day forecast, only a few ensemble members capture the evolution of the true atmosphere well.

In the area of the Great Lakes, large variations in location (east–west position) and intensity (north–south position) of the low pressure trough are observed in the six-day forecast. Figure 15 shows the corresponding probability of precipitation forecast. For areas around the Great Lakes, a high probability is predicted. This is consistent with the results in Fig. 14 where a low pressure trough is predicted to linger over these areas. However, given the uncertainty in the location and intensity of this trough, the six-day, seven-day, and eight-day precipitation forecast may not be reliable. For up to four days, however, the forecasts appear to be reliable.

We should mention that ensemble forecasting assumes that the model used for prediction is an accurate representation of the climate system. While this may not be correct (in fact different centers use different models), ensemble forecasting has become an indispensable tool in weather forecasting. With future improvements in the models and in the methods, ensemble forecasting promises to be one of the most useful operational tools ever developed in meteorology.

7. Summary

As the story goes, while chaos was discovered by a meteorologist (Edward Lorenz), the atmospheric science community ignored it completely. The seminal work of Lorenz [1963] was published in the *Journal of Atmospheric Science*, a very respectable journal published by the American Meteorological Society. It would appear that the revolutionary results of Lorenz were so far removed from the interests and focus of atmospheric scientists at that time that the paper was basically "buried". It took almost two decades for the paper to be discovered (by physicists who were eagerly looking for dynamical systems having the properties of the Lorenz system) and for the theory of chaos to emerge and develop to what many scientists consider the third revolution in science after the theories of relativity and quantum mechanics. After writing this review, I was happy to realize that we (atmospheric scientists) have, finally, redeemed ourselves.

Acknowledgments

I would like to thank Prof. David Neelin for providing Fig. 3 and Dr. Zoltan Toth for providing Figs. 14 and 15.

References

Abarbanel, H. D. I. & Kennel, M. B [1991] "Lyapunov exponents in chaotic systems: Their importance and

their evaluation using observed data," *Mod. Phys. Lett.* **B5**, 1347–1375.

Bauer, S. T. & Brown, M. B. [1992] "Empirical low-order ENSO dynamics," *Geophys. Res. Lett.* **19**, 2055–2058.

Broecker, W. S. & Denton, G. H. [1990] "What drives glacial cycles?" *Sci. Amer.* **262**, 49–56.

Buizza, R. & Palmer, T. N. [1995] "The singular vector structure of the atmospheric general circulation," *J. Atmos. Sci.* **52**, 1434–1456.

Davis, R. [1976] "Predictability of sea surface temperature and sea level pressure anomalies over the north Pacific Ocean," *J. Phys. Oceanogr.* **6**, 249–266.

Elsner, J. B. & Tsonis, A. A. [1992] "Nonlinear prediction, chaos and noise," *Bull. Amer. Meteor. Soc.* **73**, 49–60.

Elsner, J. B. & Tsonis, A. A. [1993] "Nonlinear dynamics established in the ENSO," *Geophys. Res. Lett.* **20**, 213–216.

Elsner, J. B. & Tsonis, A. A. [1996] *Singular Spectrum Analysis: A New Tool in Time Series Analysis* (Plenum, NY).

Farmer, J. D. & Sidorowich, J. J. [1987] "Predicting chaotic time series," *Phys. Rev. Lett.* **59**, 845–848.

Feder, J. [1988] *Fractals* (Plenum, NY).

Folland, C. K., Karl, T. R. & Vinnikov, K. Ya. [1990] "Observed climate variations and change," in *Climate Change: The IPCC Scientific Assessment*, eds. Houghton, J. T., Jenkins, G. I. & Ephramus, J. J. (Cambridge University Press, Cambridge), pp. 195–238.

Grassberger, P. & Procaccia, I. [1983a] "Characterization of strange attractors," *Phys. Rev. Lett.* **50**, 346–349.

Grassberger, P. & Procaccia, I. [1983b] "Measuring the strangeness of strange attractors," *Physica* **D9**, 189–208.

Hense, A. [1987] "On the possible existence of a strange attractor for the southern oscillation," *Beitr. Phys. Atmos.* **60**, 34–47.

Horel, J. D. & Wallace, J. M. [1981] "Planetary-scale atmospheric phenomena associated with the southern oscillation," *Mon. Wea. Rev.* **109**, 813–829.

Hoskins, B. J. & Karoly, J. [1981] "The steady linear response of a spherical atmosphere to thermal and orographic forcing," *J. Atmos. Sci.* **38**, 1179–1196.

Kendall, M. G. & Stuart, A. [1977] *The Advanced Theory of Statistics*,4th edition (Griffin, London).

Kuo, S., Lindberg, C. & Thomson, D. J. [1990] "Coherence established between atmospheric carbon dioxide and global temperature," *Nature* **343**, 709–714.

Lanzante, J. R. [1984] "A rotated eigenanalysis of the correlation between 700-mb heights and sea surface temperatures in the Pacific and Atlantic," *Mon. Wea. Rev.* **112**, 2270–2280.

Latif, M. & Barnett, T. P. [1994] "Causes of decadal climate variability over the North Pacific and North America," *Science* **266**, 634–637.

Latif, M. & Barnett, T. P. [1996] "Decadal climate variability over the North Pacific and North America: Dynamics and predictability," *J. Climate* **9**, 2407–2423.

Latif, M., Grotzner, A., Munnich, M., Maier-Reimer, E., Venke, S. & Barnett, T. P. [1996] "A mechanism for decadal climate variability," in *Decadal Climate Variability: Dynamics and Predictability*, eds. Davis, L. T. *et al.*, NATO ASI Series I, Vol. 44 (Springer, Berlin), pp. 263–292.

Lau, K.-M. & Chan, P. H. [1985] "Aspects of the 40–50 day oscillation during northern winter as inferred from outgoing longwave radiation," *Mon. Wea. Rev.* **113**, 1889–1909.

Lau, N. C. & Nath, M. J. [1990] "A general circulation model study of the atmosphere response to extratropical SST anomalies observed in 1950–79," *J. Climate* **3**, 965–989.

Lorenz, E. N. [1963] "Deterministic nonperiodic flow," *J. Atmos. Sci.* **20**, 130–141.

Lorenz, E. N. [1991] "Dimension of weather and climate attractors," *Nature* **353**, 241–244.

Madden, R. A. & Julian, P. R. [1971] "Detection of a 40–50 day oscillation in the zonal wind in the tropical Pacific," *J. Atmos. Sci.* **28**, 702–708.

Mandelbrot, B. B. [1983] *The Fractal Geometry of Nature* (Freeman, NY).

Molteni, F., Buizza, R., Palmer, T. N. & Petroliagis, T. [1996] "The ECMWF ensemble system: Methodology and validation," *Quart. J. R. Meteor. Soc.* **122**, 73–119.

Namias, J. [1969] "Seasonal interactions between the north Pacific Ocean and the atmosphere during the 1960s," *Mon. Wea. Rev.* **97**, 173–192.

Neelin, D. J., Battisti, D. S., Hirst, A. C. & Jin, F.-F. [1998] "ENSO theories," *J. Geophys. Res.* **103**(7), 14261–14290.

Neelin, D. J. & Latif, M. [1998] "El Niño dynamics," *Physics Today* **51**, 32–36.

Nerenberg, M. A. H. & Essex, C. [1990] "Correlation dimension and systematic geometric effects," *Phys. Rev.* **A42**, 7065–7074.

Newell, N. E., Newell, R. E., Hsiung, J. & Zhong-Xiang, W. [1989] "Global marine temperature variation and the solar magnetic cycle," *Geophys. Res. Lett.* **16**, 311–314.

Packard, N. H., Crutchfield, J. D. & Shaw, R. S. [1980] "Geometry from a time series," *Phys. Rev. Lett.* **45**, 712–716.

Priestley, M. B. [1981] *Spectral Analysis and Time Series* (Academic Press, NY).

Ruelle, D. [1981] "Chemical kinetics and differentiable dynamical systems," in *Nonlinear Phenomena in Chemical Dynamics*, eds. Pacault, A. & Vidal, C. (Springer-Verlag, Berlin), pp. 57–72.

Schneider, E. K., Huang, B. & Shukla, J. [1995]

"Ocean wave dynamics and El Niño," *J. Climate* **8**, 2414–2439.

Smith, L. A. [1988] "Intrinsic limits on dimension calculations," *Phys. Lett.* **A133**, 283–288.

Sugihara, G. & May, R. M. [1990] "Nonlinear forecasting as a way of distinguishing chaos from measurement error in time series," *Nature* **344**, 734–741.

Sun, D.-Z. & Trenberth, K. [1998] "Coordinated heat removal from the equatorial Pacific during the 1986–87 El Niño," *Geophys. Res. Lett.* **25**, 2659–2662.

Takens, F. [1981] "Detecting strange attractors in turbulence," in *Dynamical Systems and Turbulence, Lecture Notes in Mathematics*, Vol. 898, eds. Rand, D. & Young, L. S. (Springer-Verlag, Berlin), pp. 366–381.

Thomson, D. J. [1982] "Spectrum estimation and harmonic analysis," *Proc. IEEE* **70**, 1055–1096.

Toth, Z. & Kanlay, E. [1993] "Ensemble forecasting at NMC: The generation of pertubations," *Bull. Amer. Meteor. Soc.* **74**, 2317–2330.

Toth, Z. & Kanlay, E. [1995] "Ensemble forecasting at NCEP and the breeding method," NMC Office Note 407, 58 pp. [Available from NCEP, 5200 Auth. Rd., Camp Springs, MD 20746].

Trenberth, K. E. & Hurrell, J. W. [1994] "Decadal atmosphere–ocean variations in the Pacific," *Climate Dyn.* **9**, 303–319.

Trenberth, K. E. [1997] "The definition of El Niño," *Bull. Amer. Meteor. Soc.* **78**, 2771–2777.

Tsonis, A. A. & Elsner, J. B. [1988] "The weather attractor over very short time scales," *Nature* **33**, 545–547.

Tsonis, A. A. & Elsner, J. B. [1989] "Chaos, strange attractors and weather," *Bull. Amer. Meteor. Soc.* **70**, 16–23.

Tsonis, A. A. [1992] *Chaos: From Theory to Applications* (Plenum, NY).

Tsonis, A. A. & Elsner, J. B. [1992] "Nonlinear prediction as a way of distinguishing chaos from random fractal sequences," *Nature* **358**, 217–220.

Tsonis, A. A., Triantafyllou, G. N. & Elsner, J. B. [1994] "Searching for determinism in observed data: A review of the issues involved," *Nonlin. Process. Geophys.* **1**, 12–25.

Tsonis, A. A. [1996] "Dynamical systems as models for physical processes," *Complexity* **1**(5), 23–33.

Tsonis, A. A. & Elsner, J. B. [1996] "Mapping the channels of communication between the tropics and higher latitudes in the atmosphere," *Physica* **D92**, 237–244.

Tsonis, A. A. & Elsner, J. B. [1997] "Global temperature as a regulator of climate predictability," *Physica* **D108**, 191–196.

Tsonis, A. A. [1998] "Fractality in nature," *Science* **279**, 1614–1615.

Tsonis, A. A., Roebber, P. J. & Elsner, J. B. [1998] "A characteristic time scale in the global temperature record," *Geophys. Res. Lett.* **25**, 2821–2823.

Tsonis, A. A., Roebber, P. J. & Elsner, J. B. [1999] "Long-range correlations in the extratropical atmospheric circulation: Origins and implications," *J. Climate* **12**, 1534–1541.

Tziperman, E., Stone, L., Cane, M. A. & Jarosh, H. [1994] "El Niño chaos: Overlapping of reasonances between the seasonal cycle and the Pacific Ocean-atmosphere oscillator," *Science* **264**, 72–74.

UCAR Quarterly [1997] "*El Niño and Global Warming: What's the Connection?*" UCAR office of programs, Vol. 24, winter 1997.

Vallis, G. K. [1986] "El-Nino: A chaotic dynamical system?" *Science* **232**, 243–245.

Wales, D. J. [1991] "Calculating the rate of loss of information from chaotic time series by forecasting," *Nature* **350**, 485–488.

Wallace, J. M. & Gutzler, D. S. [1981] "Teleconnections in the geopotential height field during the Northern Hemisphere winter," *Mon. Wea. Rev.* **109**, 784–817.

Wallace, J. M. & Jiang, Q. R. [1987] "On the observed structure of the interannual variability of the atmosphere/ocean climate system," in *Atmospheric and Oceanic Variability*, ed. Cattle, H. (Royal Meteorological Society, London), pp. 17–43.

Wallace, J. M., Smith, C. & Jiang, Q. R. [1990] "Spatial patterns of atmosphere ocean interactions in the northern winter," *J. Climate* **3**, 990–988.

Wiin-Nielsen, A. & Chen, T.-C. [1993] *Fundamentals Atmospheric Energetics* (Oxford, NY).